ELSEVIER

Microporous and Mesoporous Materials 48 (2001) 111–118

MICROPOROUS AND MESOPOROUS MATERIALS

www.elsevier.com/locate/micromeso

EPR spectroscopy of copper and manganese complexes encapsulated in zeolites

T.H. Bennur, D. Srinivas, Paul Ratnasamy *

National Chemical Laboratory, Pune 411 008, India

Received 6 August 2000; received in revised form 14 November 2000; accepted 27 November 2000

Abstract

The structural basis for the enhanced catalytic activities of copper and manganese Schiff base complexes encapsulated in zeolite-Y is investigated by EPR spectroscopy. The study provides an unequivocal evidence for the encapsulation of complexes inside the supercages of zeolite-Y. The EPR spectroscopy distinguishes the encapsulated complexes from the ''neat'' and surface-adsorbed metal complexes. Neat complexes showed broad EPR spectra corresponding to nearest neighbour spin–spin interactions whereas the zeolite-encapsulated metal complexes showed well resolved metal hyperfine features similar to the spectra in dilute frozen solutions. The spin Hamiltonian parameters reveal a distorted square pyramidal geometry and an increase in the in-plane covalency of metal–ligand bond as a consequence of encapsulation. The observed changes in the molecular electronic structure are correlated to the enhanced catalytic activity of the encapsulated metal complexes.

Keywords: Zeolite-encapsulated metal complexes; Zeozymes; Ship-in-a-bottle complexes; EPR spectroscopy; Copper complexes; Manganese complexes; Schiff base complexes; Structure; Oxidation catalysts

1. Introduction

Transition metal complexes encapsulated in the pores and void spaces of zeolites and zeolitic materials have been receiving special attention as inorganic mimics of enzymes [1–3]. While the metal complex imitates the role of the active site, the zeolite mantle presumably replaces the surrounding protein moiety of metalloenzymes. The ''zeozymes'' (*acronym* for zeolite mimics of enzymes) possess dual advantages of the heterogeneous catalysts (like easy catalyst separation, ruggedness, etc.) as well as the homogeneous catalysts (like a well-defined, unique structure which can be elucidated and correlated with the activity). We have found that the intrinsic catalytic activity of zeolite-encapsulated metal acetato, phthalocyanine and Schiff base complexes was enhanced significantly in the selective oxidation of aliphatic and aromatic hydrocarbons, hydroxylation of phenols, epoxidation of olefins, oxyhalogenation of aromatic compounds and decomposition of H_2O_2 and *tert*-butyl hydroperoxide [4–7]. In continuation of our efforts in understanding the structural origin of this enhanced catalytic activity (and, in some cases, the selectivity) [7–9] we report here EPR investigations of copper and manganese Schiff

* Corresponding author. Tel.: +91-20-5893030; fax: +91-20-5893355.

E-mail address: prs@ems.ncl.res.in (P. Ratnasamy).

1387-1811/01/$ - see front matter
PII: S1387-1811(01)00345-6

base salen and saloph complexes encapsulated in zeolite NaY. EPR spectroscopy is ideal to probe both molecular and electronic structural information of the paramagnetic ions and the effect of molecular confinement on the conformational geometry and mobility of the complexes inside the zeolitic cages. We demonstrate that EPR spectroscopy can be used to distinguish and estimate independently the encapsulated complexes from those adsorbed on the external surface.

2. Experimental

2.1. Synthesis of neat complexes

In the preparation of Cu(salen) and Cu(saloph), where salen = *N*,*N*′-ethylenebis(salicylidenaminato) and saloph = *N*,*N*′-*o*-phenylenebis(salicylidenaminato), the corresponding Schiff base ligand (5 mM) was taken in 20 ml of methanol. To a boiling solution of this, $Cu(CH_3COO)_2 \cdot 2H_2O$ (5 mM) dissolved in 15 ml of methanol was added slowly, over a period of 30 min. The reaction mixture was refluxed for 3–4 h and cooled to 298 K. The solid complexes were filtered and recrystallized from methanol.

Mn(salen) and Mn(saloph) complexes were prepared in a similar manner, using $Mn(CH_3COO)_2 \cdot 4H_2O$. The reactions were carried out under argon atmosphere.

2.2. Synthesis of encapsulated copper and manganese complexes

Zeolite-Y-encapsulated copper and manganese Schiff base complexes, Cu(salen)–Y, Cu(saloph)–Y, Mn(salen)–Y and Mn(saloph)–Y, were prepared by the "flexible ligand" method [8]. In this method, Cu(II) and Mn(II)-exchanged zeolite Na–Y (1.2 wt.%) were, first, prepared. The samples were dehydrated and thoroughly mixed with the corresponding Schiff base ligand (ligand:metal = 3:1). The mixture was heated first to 373 K for 1 h and then, to 523 K. The heating was continued for 5–6 h. The formation of the product was observed by a change in colour of the substance from cream to brown. The free ligand was removed by Soxhlet extraction with chloroform, acetonitrile and finally, with acetone for two days.

In the case of manganese complexes encapsulated in zeolites the preparation was carried out under nitrogen atmosphere to prevent oxidation of Mn(II) to Mn(III).

2.3. Physical measurements

The physico-chemical characterizations of the neat and encapsulated complexes were done as described earlier [6,8]. EPR spectra were recorded on a Bruker EMX X-band spectrometer operating at 100 kHz field modulation. The microwave frequency was calibrated using a frequency counter fitted in the microwave bridge ER 041 XG-D. The measurements at 77 K were performed using a quartz finger Dewar. Spectral simulations were carried out by means of the Bruker Simfonia software package.

3. Results and discussion

The elemental compositions (Table 1) confirmed the purity and stoichiometry of the neat and zeolite-encapsulated complexes. No major changes, except a marginal reduction in peak intensity, were observed in the X-ray diffraction patterns of zeolite-Y indicating that encapsulation of complexes did not alter the zeolite framework structure. The colour of the complexes changed on encapsulation. Neat Cu(salen), which was green, became brick red on encapsulation. Similarly, reddish brown Mn(saloph) became yellowish green on encapsulation.

The IR spectra of the encapsulated metal complexes were weak and masked by the zeolite bands due to the low concentration of the former. The assignments of a few representative IR bands are listed in Table 1. The neat complexes showed a sharp band in the range 1600–1650 cm^{-1} attributable to the stretching mode of the azomethine group (ν(C=N)). A strong band corresponding to ν(C=C) appeared in the range 1577–1597 cm^{-1}. The ring vibrations and C–O stretching modes appeared in the ranges 1440–1540 and 1284–1340 cm^{-1}, respectively. In Cu(saloph) the band corre-

Table 1
Chemical composition and IR stretching frequencies of neat and zeolite-encapsulated copper and manganese Schiff base complexes

Complex	Chemical composition[a] (%)				IR data (cm^{-1})				Colour
	C	H	N	C/N	ν(C=N)	ν(C=C)	Ring	ν(C–O)	
Cu(salen)·CH_3OH-neat	56.0 (56.4)	4.7 (5.0)	7.5 (7.7)	7.5 (7.3)	1647, 1629	1596	1541, 1496	1304	Green
Cu(salen)–Y	9.05	2.18	1.37	6.6 (6.9)					Brick red
Cu(saloph)·0.5CH_3OH-neat[b]	62.4 (62.3)	4.4 (4.1)	7.2 (7.1)	8.7 (8.6)	1608	1577	1521, 1460	1339	Brick red
Cu(saloph)–Y	10.1	1.3	1.6	6.4 (8.6)					Brick red
Mn(salen)-neat	60.0 (59.8)	4.4 (4.4)	8.2 (8.7)	7.3 (6.9)	1627	1598	1541, 1496	1284	Brown
Mn(salen)–Y	10.8	1.4	1.2	9.3 (6.9)					Brick red
Mn(saloph)·CH_3OH-neat	61.1 (60.0)	4.4 (4.5)	6.4 (6.9)	9.5 (8.6)	1627	1597	1541, 1496	1284	Reddish brown
Mn(saloph)–Y					[c]	1566	1537, 1490	1275	Yellowish Green

[a] Estimated values are given in parentheses.
[b] Neat Cu(saloph) in solid state is associated with half molecule of CH_3OH as solvent of crystallization.
[c] Overlaps with zeolite framework bands.

sponding to ν(C=N) shifted from 1647 cm^{-1} (in salen) to 1608 cm^{-1}. Similar low energy shifts were observed also for ν(C=C) and the ring vibrational modes. The band corresponding to the ν(C–O) vibration shifted from 1304 cm^{-1} in Cu(salen) to 1339 cm^{-1} in Cu(saloph). These shifts in band positions are consistent with changes in X-ray structural parameters reported earlier [10,11]. The IR spectra reveal that the band due to ν(C–O) shifts to lower values in the manganese compared to copper complexes. These results reveal that the metal–ligand bond is more covalent in Cu(II) than in Mn(II) complexes.

3.1. EPR of Cu(II) and Mn(II) exchanged NaY

The EPR spectrum of Cu(II) exchanged NaY (1.2 wt.%) revealed two types of species: Species I (characterized by a low-symmetry environment with $g_x = 2.083$, $g_y = 2.095$ and $g_z = 2.373$ and $A_x = A_y = 14.5$ G and $A_z = 118.4$ G) corresponding to Cu(II) ions located at the hexagonal prism and species II (exhibiting dynamic Jahn–Teller effect with $g_{av} = 2.181$) corresponding to the ions in the supercages (Fig. 1(a)). Mn(II) exchanged Na–Y (1.2 wt.%) showed a six line spectrum ($g_{iso} = 2.0$) arising from the transitions between $|+1/2\rangle$ and $|-1/2\rangle$ electron spin levels of manganese and due to coupling of electron spin with ^{55}Mn nucleus spin ($S = 5/2$, $I = 5/2$) (Fig. 1(b)). The other zero-field transitions corresponding to $m_S = |\pm 5/2\rangle \leftrightarrow |\pm 3/2\rangle$ and $|\pm 3/2\rangle \leftrightarrow |\pm 1/2\rangle$ contributed to the background upon which the six major hyperfine resonances were superimposed. The spectra also revealed five weak doublets (Fig. 1(c), marked by arrows) attributable to $\Delta M_I = \pm 1$ (forbidden) transitions and a low-symmetry molecular environment at Mn(II) as in the case of Cu(II) exchanged samples (species I).

3.2. EPR of neat and encapsulated copper complexes

The powder samples of neat Cu(salen) and Cu(saloph) showed spectra characterized by axial g tensors (Fig. 2(a) and (b), respectively). The hyperfine features due to copper ($S = 1/2$, $I = 3/2$) could not be resolved, even at 77 K, due to intermolecular spin–spin interactions. This observation is in accordance with the dimeric association of these molecules in the solid state [10,11]. Cu(salen) has a square pyramidal geometry while

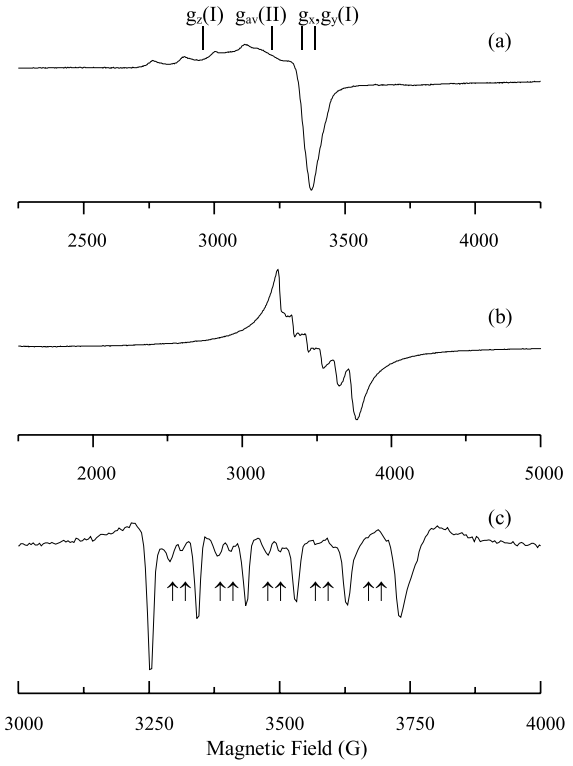

Fig. 1. X-band EPR spectra of Cu(II) and Mn(II) exchanged NaY (1.2 wt.%) at 298 K: (a) Cu–Y, (b) Mn–Y and (c) second derivative plot of Mn–Y. Arrows represent the "forbidden" transitions.

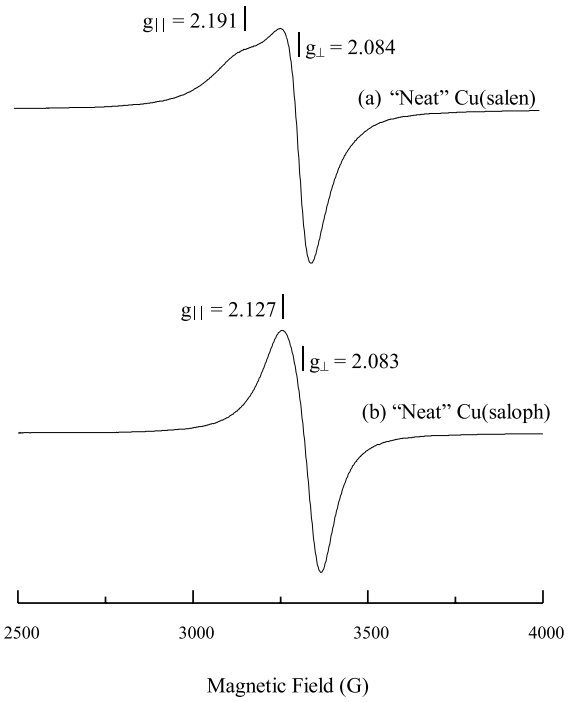

Fig. 2. EPR spectra (at 298 K) for the polycrystalline samples of neat Cu(salen) (a) and Cu(saloph) (b).

Cu(saloph) is square planar. These structural differences are manifested on the spectral features (Fig. 2) and the g values (Table 2).

The intermolecular spin–spin interactions were removed in frozen solutions and as a consequence of this, the copper hyperfine splitting was resolved. Typical spectra for Cu(saloph) in $CHCl_3$ and pyridine are shown in Fig. 3(a) and (b). The well resolved superhyperfine features in Fig. 3(a) are due to magnetically equivalent nitrogen nuclei of the saloph ligand. These features could not be resolved in strong donor solvents like pyridine (Fig. 3(b)), perhaps due to changes in the conformational geometry of the Schiff base moiety. The saloph complex adopts a planar geometry in $CHCl_3$ and a square pyramidal geometry in pyridine solutions [10,11].

The spin Hamiltonian parameters for frozen solutions of Cu(II), obtained after spectral simulations, are listed in Table 2. Solvents exerted a marked effect on the g and A values of the complexes. The $g_\parallel$ value increases while $A_\parallel$ decreases with increasing σ-donation capacity of the solvent. For example, the $g_\parallel$ value of 2.183 for Cu(saloph) in $CHCl_3$ increases to 2.227 in pyridine. In strong donor solvents like DMF and pyridine, the solvent molecule coordinates to Cu(II) forming a square pyramidal geometry. A comparison of values for Cu(salen) and Cu(saloph) reveal that due to the additional phenyl ring, Cu(saloph) forms a more stable square pyramidal complex than Cu(salen) ($g_\parallel$ value varies in the order Cu(saloph) > Cu(salen)). The $A_\parallel$ value in pyridine solvent varies in the order Cu(saloph) < Cu(salen) indicating the greater electron delocalization to ligand orbitals in Cu(saloph) than in Cu(salen).

The spectra for the zeolite-Y-encapsulated copper complexes, Cu(salen)–Y and Cu(saloph)–Y are characterized by an axial spin Hamiltonian (Fig. 3(c)). A comparison of Figs. 1(a) and 3(c) confirms that all the exchanged Cu(II) ions in

Table 2
EPR spin Hamiltonian parameters of neat and zeolite-encapsulated Cu(II) and Mn(II) Schiff base complexes at 77 K

Complex 0	State	$g_{\parallel}$	$g_{\perp}$	$-A_{\parallel}$ (G)	$-A_{\perp}$ (G)	$A_{\parallel}^{N}$ (G)	g_{av}	A_{av} (G)	D cm^{-1}
Cu(salen)	Neat	2.191	2.084	NR	NR	NR			
	$CHCl_3/CH_3OH$ (1:3)	2.199	2.067	199.4	26.0	10.8			
	DMF	2.210	2.053	195.3	30.3	NR			
	Pyridine	2.225	2.053	191.3	24.0	NR			
Cu(salen)–Y	Encapsulated	2.269	2.051	163.3	28.6	NR			
Cu(saloph)	Neat	2.127	2.083	NR	NR	NR			
	$CHCl_3$	2.183	2.032	115.0	15.0	15.2			
	CH_3OH	2.223	2.066	193.0	15.3	NR			
	DMF	2.216	2.060	197.0	31.5	12.6			
	Pyridine	2.227	2.065	187.3	22.6	NR			
Cu(saloph)–Y	Encapsulated	2.282	2.061	160.0	29.1	NR			
Mn–Y							2.000	97.6	
Mn(salen)	Neat						2.000		0.12
Mn(saloph)	Neat						2.012	NR	
	CH_3OH						1.998	96.0	
	Pyridine						1.999	92.0	0.09
Mn(saloph)–Y	Encapsulated						1.997	94.6	0.08

NR: not resolved; $A_{\parallel}^{N}$ refers to the parallel component of the superhyperfine coupling due to nitrogen.

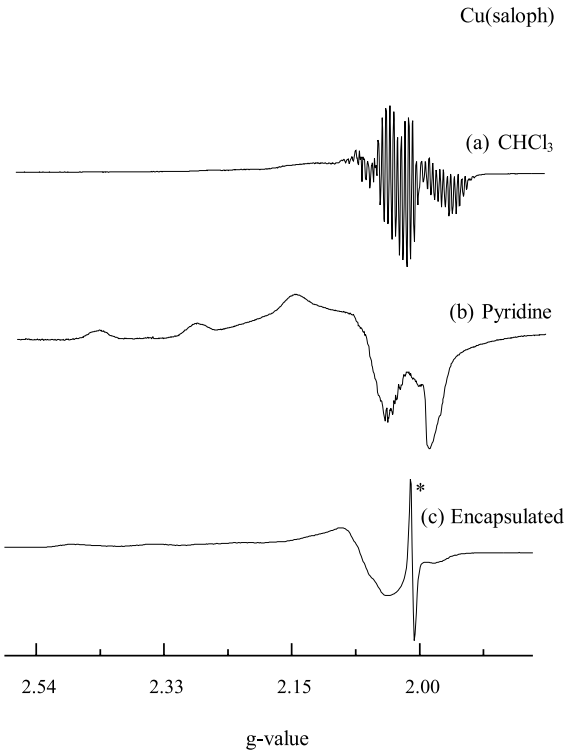

Fig. 3. EPR spectra of Cu(saloph) at 77 K: (a) in $CHCl_3$, (b) in pyridine, and (c) zeolite-encapsulated Cu(saloph). Asterisk corresponds to signal due to free radical.

zeolite were complexed. The spectra of the encapsulated complexes (Fig. 3(c)) resemble those of the frozen solutions (Fig. 3(b)) rather than the neat complexes (Fig. 2(a)). The resolution in the copper hyperfine features confirm that the encapsulated metal complexes are isolated and present as monomeric species. The higher $g_{\parallel}$ (2.269 for Cu(salen)–Y and 2.282 for Cu(saloph)–Y) and lower $A_{\parallel}$ (163.3 G for Cu(salen)–Y and 160.0 G for Cu(saloph)–Y) values of the encapsulated complexes suggest square pyramidal geometry for copper. While the Schiff base ligand provides quadridentate coordination, the zeolite framework (hexagonal prism) provides a strong axial coordination. The spectrum for the surface-adsorbed copper complex is almost similar to the neat complex (Fig. 2). Hence, EPR spectroscopy can be used to differentiate the zeolite-encapsulated complexes from the surface-adsorbed complexes.

3.3. EPR of neat and encapsulated manganese complexes

Fig. 4 depicts the EPR spectra of neat manganese complexes. Mn(salen) showed the five, zero-field transitions. The zero-field splitting parameter

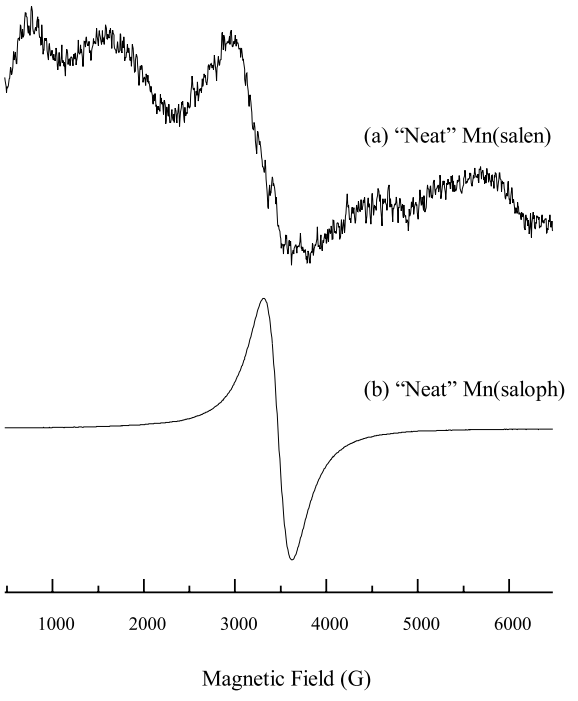

Fig. 4. EPR spectra for the polycrystalline samples of neat (a) Mn(salen) and (b) Mn(saloph) at 298 K.

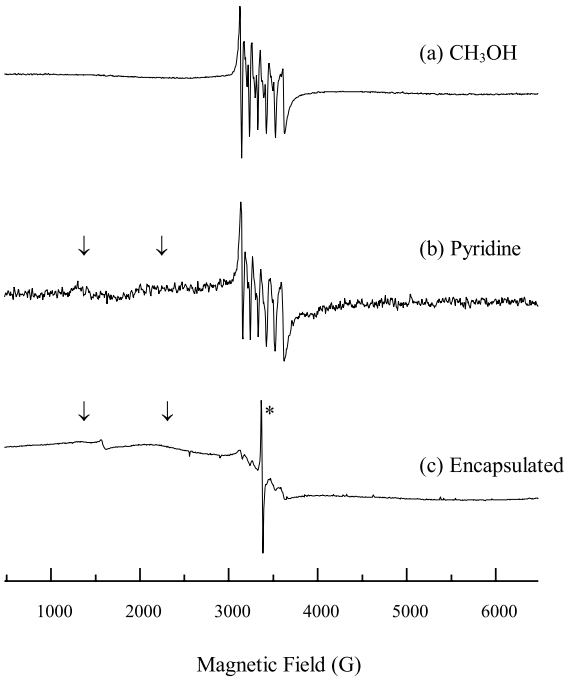

Fig. 5. EPR spectra of Mn(saloph) at 77 K: (a) in CH_3OH, (b) in pyridine, and (c) zeolite-encapsulated Mn(saloph) complex. Asterisk corresponds to signal due to free radical.

(D) was estimated to be 0.12 cm^{-1}. Unlike in Mn–Y, the manganese hyperfine features could not be resolved. In contrast, Mn(saloph), showed only a single isotropic resonance at $g = 2$. The intermolecular exchange interactions in Mn(saloph) are, hence, larger than the zero-field interaction (>0.12 cm^{-1}). These interactions in Mn(salen) are an order of magnitude lower than that in Mn(saloph) (>0.009 cm^{-1}).

Frozen solutions showed resolved Mn(II) hyperfine features. Typical spectra for Mn(saloph) in methanol and pyridine are shown in Fig. 5(a) and (b), respectively. The forbidden transitions ($\Delta m_S = \pm 1$ and $\Delta M_I = \pm 1$) are also visible. In pyridine solutions, the zero-field transitions (marked by arrows) are more prominent than in methanol, probably due to higher zero-field interactions ($D =$ 0.087 cm^{-1}) and the tetragonally elongated square pyramidal geometry. It is interesting to note that the intensity of Mn(II) signal decreased in pyridine solutions, probably due to solvent promoted Mn(II) to Mn(III) oxidation.

Before complexation, Mn–Y samples showed a sextet pattern with a total spectral width of 520 G. After the complex formation, in zeolites, the spectrum extends over a wider field range and displays fine splitting (marked by arrows, Fig. 5(c)). The spectra of the zeolite-encapsulated Mn(II) Schiff base complexes are similar to that of frozen solutions (Fig. 5(b) and (c)). The weak sharp signal at 1600 G corresponds to Fe(III) impurity in NaY while the intense signal (denoted by an asterisk) overlapping with the Mn sextet lines corresponds to a free radical. The similarity of zeolite-encapsulated complexes and frozen Mn(II) solutions (as in the case of copper complexes) suggests that manganese complexes encapsulated in zeolites are isolated and present as monomers. The hyperfine coupling constants of zeolite-encapsulated and pyridine-solvated Mn(II) complexes are lower than that of the methanol solution and Mn–Y. The zero-field splitting parameter (D) for the encapsulated complexes is similar to that of the pyridine-solvated complex

suggesting that the geometry of Mn(II) complexes in pyridine solutions and in zeolite-Y are distorted. The Mn–ligand bond was more covalent, the metal electron density being partially delocalized onto the ligand orbitals.

3.4. Electronic structure and bonding parameters

The molecular symmetry of the Schiff base complexes is low (C_{2v}). In such a case, the EPR spectra of these complexes should be characterized by three g parameters g_x, g_y and g_z. However, as seen in the previous section the spectra of copper complexes are characterized only by axial g and hyperfine tensors $g_\parallel$ and $g_\perp$ and $A_\parallel$ and $A_\perp$). This implies that although the molecular symmetry is low, the electronic symmetry at the site of metal ion is as high as C_{4v}. The g values for the copper complexes, with $g_\parallel > g_\perp$ indicate that the unpaired electron of Cu occupies the $3d_{x^2-y^2}$ orbital. The ground state electronic wave function and the bonding parameters were evaluated using the ligand field approach described in our previous paper [7]. Here α and β are the metal d-orbital coefficients for the MOs b_{1g} and b_{2g} representing the in-plane σ and π bonding, respectively; δ is the coefficient for the MO e_g representing the out-of-plane π bonding; α' is the coefficient for the ligand orbitals forming b_{1g} molecular orbital. The MO coefficients estimated from the experimental g and A values are listed in Table 3.

The MO coefficient are, in general, smaller than unity indicating the covalent nature of the bonding between the metal and ligand orbitals. UV–VIS spectra showed a band in the range 16,420–17,825 cm^{-1} corresponding to the excitation transition of $B_{1g} \leftrightarrow A_g$. The band corresponding to $B_{1g} \leftrightarrow E_g$ could not be resolved. Thus the value of δ (coefficient for out-of-plane π bonding) could not be estimated, but evaluated in units of energy separation.

In general, the MO coefficients varied in the order $\beta < \alpha$ suggesting that the in-plane π-bonding (between $3d_{xy}$ and p_π orbitals) is more covalent than the in-plane σ-bonding (between $3d_{x^2-y^2}$ and p_σ orbitals). The MO coefficients are modified considerably on encapsulation. The coefficient α, characteristic of in-plane σ bonding, decreases while β, characteristic of in-plane π-bonding, increases on encapsulation. These results reveal the structural changes undergone by the metal complex on encapsulation. The higher in-plane covalency as indicated by smaller values of α for encapsulated metal complexes (α changes from 0.836 to 0.812 for Cu(salen) and 0.847 to 0.821 for Cu(saloph)) reveals a larger depletion of electron density at the site of metal in encapsulated complexes than in neat complexes. *This depletion in turn is likely to facilitate nucleophilic attacks by reagents like the tert-butyl hydroperoxide or hydrogen peroxide anions at the metal centre.* Since the transition metal hydroperoxides are transient species in the oxidative catalysis, *an enhancement in their rates of formation will increase the catalytic activity*. The in-plane covalency appears to be higher in salen than in saloph complexes. Even in

Table 3
Molecular orbital coefficients and electronic d–d transition energies for neat and encapsulated copper Schiff base complexes

Complex	State	MO coefficients				d–d transition energies (cm^{-1})
		α^2	α'^2	β^2	$\delta^2/\Delta E_{xz/yz} \times 10^5$	$E_{xy} - E_{x^2-y^2}$
Cu(salen)	CH_3Cl/CH_3OH	0.836	0.249	0.661	4.91	17,730
	DMF	0.832	0.253	0.687	3.86	17,361
	Pyridine	0.839	0.249	0.705	3.83	16,750
Cu(salen)–Y	Encapsulated	0.812	0.277	0.910	3.82	17,391
Cu(saloph)	CH_3OH	0.847	0.236	0.734	4.76	17,825
	DMF	0.845	0.236	0.701	4.31	17,793
	Pyridine	0.835	0.250	0.699	5.44	16,420
Cu(saloph)–Y	Encapsulated	0.821	0.266		4.54	

the manganese complexes the hyperfine coupling constant decreases from 97.6 to 94.6 G on encapsulation and suggest a similar depletion of spin density at the site of the metal ion in encapsulated complexes. Hence, a smaller value of α, increased in-plane covalency and reduced hyperfine coupling constants are the likely causes for the enhanced catalytic activity of the encapsulated complexes.

4. Conclusions

EPR spectroscopy has been used to provide an unequivocal evidence for the encapsulation of copper and manganese Schiff base salen and saloph complexes inside the supercages of zeolite-Y. EPR spectroscopy has distinguished the encapsulated complexes from the neat and surface-adsorbed complexes. While the spectra of surface-adsorbed complexes resembled those of neat solid complexes, the spectra of the encapsulated complexes are similar to those of frozen solutions. The effect of encapsulation is manifested on molecular structural and geometric changes. *Our EPR spectroscopic studies suggest that the distortion in molecular geometry arising out of encapsulation and the consequent depletion of electron density at metal site are the probable causes for the enhanced catalytic activity of the zeolite-encapsulated copper and manganese complexes.*

Acknowledgements

One of the authors (T.H.B.) thanks Council of Scientific and Industrial Research, New Delhi for the award of Senior Research Fellowship.

References

[1] K.J. Balkus Jr., A.G. Gabrielov, J. Incl. Phenom. Mol. Recog. Chem. 21 (1995) 159.
[2] D.E. De Vos, J.L. Meinershagen, T. Bein, Angew. Chem. Int. Ed. Engl. 35 (1996) 2211.
[3] M.J. Sabater, A. Corma, A. Domenech, V. Fornes, H. Garcia, J. Chem. Soc. Chem. Commun. (1997) 1285.
[4] R. Raja, P. Ratnasamy, J. Catal. 170 (1997) 244.
[5] R. Raja, P. Ratnasamy, Catal. Lett. 48 (1997) 1.
[6] C.R. Jacob, S.P. Varkey, P. Ratnasamy, Micropor. Mesopor. Mater. 22 (1998) 465.
[7] S. Deshpande, D. Srinivas, P. Ratnasamy, J. Catal. 188 (1999) 261.
[8] S. Chavan, D. Srinivas, P. Ratnasamy, Topics Catal. 11/12 (2000) 359.
[9] S. Chavan, D. Srinivas, P. Ratnasamy, J. Catal. 192 (2000) 286.
[10] M.M. Bhadbhade, D. Srinivas, Inorg. Chem. 32 (1993) 5458.
[11] E. Suresh, M.M. Bhadbhade, D. Srinivas, Polyhedron 15 (1996) 4133.